Epstein-Barr virus nuclear antigen 2 (EBNA2) extensively rewires the human chromatin landscape at autoimmune risk loci

Ted Hong[1,2], Omer Donmez[1], Daniel Miller[1], Carmy Forney[1], Michael Lape[1,3], Sreeja Parameswaran[1], Mariana Saint Just Ribeiro[1], Jun Liang[4], Albert Magnusen[5], William Miller[6], Iouri Chepelev[1,7], John B. Harley[1,7,8], Bo Zhao[4] , Leah C. Kottyan[#1,7,9,10], Matthew T. Weirauch[#1,3,7,11]

[#] Co-corresponding authors: Leah.Kottyan@cchmc.org; Matthew.Weirauch@cchmc.org

[1] Center for Autoimmune Genomics and Etiology, Cincinnati Children's Hospital Medical Center, Cincinnati, Ohio, USA, 45229.

[2] Department of Pharmacology & Systems Physiology, University of Cincinnati, College of Medicine, Cincinnati, Ohio, USA, 45229.

[3] Division of Biomedical Informatics, Cincinnati Children's Hospital Medical Center, Cincinnati, Ohio, USA, 45229.

[4] Department of Medicine, Brigham and Women's Hospital, Harvard Medical School, Boston, MA 02115.

[5] Division of Human Genetics, Cincinnati Children's Hospital Medical Center, Cincinnati, Ohio, USA, 45229.

[6] Department of Molecular Genetics, Biochemistry, and Microbiology, University of Cincinnati, College of Medicine, Cincinnati, Ohio, USA, 45267.

[7] Department of Pediatrics, University of Cincinnati, College of Medicine, Cincinnati, Ohio, USA, 45229.

[8] US Department of Veterans Affairs Medical Center, Cincinnati, Ohio 45229, USA

[9] Division of Immunobiology, Cincinnati Children's Hospital Medical Center, Cincinnati, Ohio, USA, 45229.

[10] Division of Allergy and Immunology, Cincinnati Children's Hospital Medical Center, Cincinnati, Ohio, USA, 45229.

[11] Division of Developmental Biology, Cincinnati Children's Hospital Medical Center, Cincinnati, Ohio, USA, 45229.

Running Title: EBNA2 rewires the human genome at autoimmune loci

Key words: gene regulation, functional genomics, virology, autoimmune disease, genetic risk

Abstract

The interplay between environmental and genetic factors plays a key role in the development of many autoimmune diseases. In particular, the Epstein-Barr virus (EBV) is an established contributor to multiple sclerosis, lupus, and other disorders. Previously, we demonstrated that the EBV nuclear antigen 2 (EBNA2) transactivating protein occupies up to half of the risk loci for a set of seven autoimmune disorders. To further examine the mechanistic roles played by EBNA2 at these loci on genome-wide scale, we globally examined gene expression, chromatin accessibility, chromatin looping, and EBNA2 binding, in a B cell line that was 1) uninfected, 2) infected with a strain of EBV lacking EBNA2, or 3) infected with a strain that expresses EBNA2. We identified >400 EBNA2-dependent differentially expressed human genes and >4,000 EBNA2 binding events in the human genome. ATAC-seq analysis revealed >3,000 regions in the human genome with EBNA2-dependent chromatin accessibility, and HiChIP-seq data revealed >2,000 regions where EBNA2 altered chromatin looping interactions. Importantly, autoimmune genetic risk loci were highly enriched at the sites of these EBNA2-dependent chromatin-altering events. We present examples of autoimmune risk genotype-dependent EBNA2 events, nominating genetic risk mechanisms for autoimmune risk loci such as *ZMIZ1* and *CD80*. Taken together, our results reveal important interactions between host genetic variation and EBNA2-driven disease mechanisms. Further, our study highlights a critical role for EBNA2 in rewiring human gene regulatory programs through rearrangement of the chromatin landscape and nominates these interactions as components of genetic mechanisms that influence the risk of multiple autoimmune diseases.

Introduction

Crosstalk between genetic risk polymorphisms and environmental factors is thought to influence the onset and progression of many human diseases (Hunter 2005; Bookman et al. 2011; McAllister et al. 2017). Many diseases have a complex genetic etiology, including cancers (Flavahan et al. 2017), cardiovascular diseases (North et al. 2003), and autoimmune diseases such as multiple sclerosis (MS) (Ascherio and Munger 2007) and systemic lupus erythematosus (SLE) (Kamen 2014). Over the past 15 years, a multitude of genome-wide association studies (GWASs) have identified more than 50,000 disease-associated genetic variants for many disorders (Tam et al. 2019). As many as 90% of disease-associated genetic variants fall within non-coding regions of the genome (Hindorff et al. 2009; Maurano et al. 2012), implicating a key role for regulatory proteins such as transcription factors (TFs) in the etiology of human disease (Lee and Young 2013; Deplancke et al. 2016). Regulatory proteins bind promoter regions and distal regions of target genes (e.g., enhancers) to alter gene expression through numerous mechanisms (reviewed in (Lambert et al. 2018; Sullivan et al. 2018; Schoenfelder and Fraser 2019)). Some regulatory proteins, such as the pioneer factor EBF1, are capable of directly altering the chromatin landscape. Other TFs, such as YY1 and CTCF, can affect the three-dimensional structure of chromatin by facilitating the formation of novel chromatin loops that alter gene transcription (Beagan et al. 2017; Weintraub et al. 2017). Thus, regulatory proteins likely can contribute to human disease processes through a variety of mechanisms.

Viral infections are a common environmental exposure known to be closely linked to many human diseases (Bray et al. 1983; Foxman and Iwasaki 2011; Hong et al. 2014; Pender and Burrows

2014). In particular, previous studies have revealed causative roles for the Epstein-Barr virus (EBV) in mononucleosis (Dunmire et al. 2015), Burkitt's lymphoma (Rochford and Moormann 2015), and Hodgkin lymphoma (Vockerodt et al. 2014). EBV is also strongly implicated in autoimmune diseases such as rheumatoid arthritis (RA) (Balandraud and Roudier 2018), inflammatory bowel disease (IBD) (Dimitroulia et al. 2013), SLE (Harley and James 2006), and MS (Bagert 2009). Despite extensive epidemiologic and serological evidence, the molecular mechanisms through which EBV-host interactions increase autoimmune disease risk remain largely unknown.

Viruses can directly perturb the host's transcriptome through the actions of virus-encoded transcriptional regulatory proteins (Agudelo-Romero et al. 2008; Clyde and Glaunsinger 2010; Bermudez-Morales et al. 2011; Graham 2016; Harley et al. 2018). Viral transcriptional regulators can either interact with the host genome directly, as is the case for the EBV-encoded Zta protein (Flemington and Speck 1990; Mahot et al. 2003), or indirectly through interactions with host DNA-binding factors, such as the EBV-encoded Epstein-Barr virus nuclear antigen 2 (EBNA2) protein and the human TF RBPJ (Henkel et al. 1994). In both cases, genetic variation in the host genome can affect these virus-host interactions, leading to alteration of host gene expression levels (Bochkov et al. 2010; Caliskan et al. 2015; Harley et al. 2018).

EBNA2 controls multiple processes, including the immortalization of EBV-infected B cells, by altering the expression levels of human genes (Pich et al. 2019). Mechanistically, EBNA2 mediates at least some of this regulation through interactions with human TFs such as RBPJ, SPI1 (PU.1), and EBF1 (Zhao et al. 2011). The EBF1 protein can bind to and open chromatin that is occupied

by EBNA2-RBPJ complexes (Lu et al. 2016). EBNA2 can also recruit chromatin remodelers such as histone acetyltransferase p300/CBP (Wang et al. 2000; Lu et al. 2016) and the SWI/SNF complex (Wu et al. 2000), further supporting a role for EBNA2 in human chromatin rearrangement. Likewise, the EBNA2-RBPJ complex can create a new chromatin looping interaction between a distal enhancer region and the *MYC* promoter, inducing *MYC* expression that leads to continuous B cell proliferation (Zhao et al. 2011; Wood et al. 2016; Jiang et al. 2017). Despite these strong independent lines of evidence implicating EBNA2 in the alteration of chromatin accessibility and looping in the human genome, a genome-wide investigation of EBNA2-dependent human chromatin alteration has not been previously performed.

A recent study from our group revealed that a significant number of autoimmune disease-associated genetic loci contain genetic variants that are located within EBNA2 ChIP-seq peaks (Harley et al. 2018). In particular, nearly half of the SLE and MS genetic risk loci contain disease-associated genetic variants that are directly located within regions of the human genome occupied by EBNA2. We also discovered numerous examples of autoimmune-associated genetic variants that alter the binding of EBNA2 and other transcriptional regulators to the human genome in a genotype-dependent manner. Collectively, these results are consistent with EBNA2 playing an important role in autoimmune disease etiology.

Understanding the molecular mechanisms mediating interactions between EBNA2 and the human genome is important for achieving an understanding of the development and progression of autoimmune diseases. In this study, we explore the role of EBNA2 within the human B cell gene regulatory network by examining EBNA2-dependent alterations to the human chromatin landscape and investigating the impact of autoimmune disease-associated genetic polymorphisms

on these mechanisms. To identify EBNA2-dependent effects, we employ an experimental design comparing human B cells that are either 1) uninfected, 2) infected with an EBV strain that lacks EBNA2 (EBV^{EBNA2-}), or 3) infected with an EBV strain that has EBNA2 (EBV^{EBNA2+}). Using RNA-seq and EBNA2 ChIP-seq data, we identify ~400 human genes whose change in expression levels coincides with the presence EBNA2. Next, we resolve the effects of EBNA2 on chromatin accessibility using Assay for Transposase-Accessible Chromatin sequencing (ATAC-seq) and chromatin looping using protein-centric chromatin conformation sequencing (HiChIP-seq), revealing EBNA2-dependent changes in chromatin accessibility (~3000 genomic regions), and chromatin looping (~2000 regions). We observe striking enrichment for autoimmune disease risk genetic variants within many of these EBNA2-dependent regulatory mechanisms. We also identify allele-dependent EBNA2 behavior at >20 autoimmune-associated variants. Our discovery of genome-wide EBNA2-dependent perturbations of the human transcriptome through alterations to the human chromatin landscape reveals an important molecular mechanism possibly underlying the onset and progression of multiple autoimmune diseases.

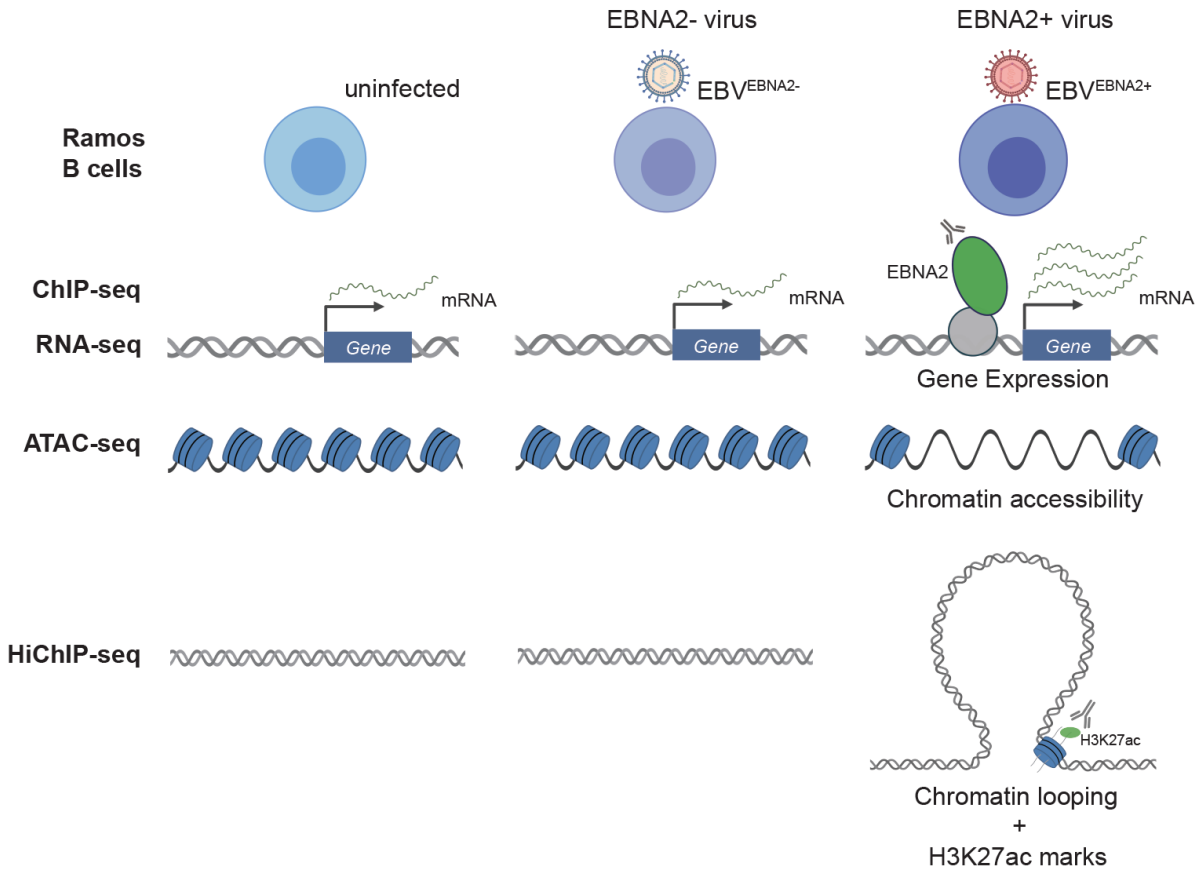

Figure. 1. Schematic overview of the experimental design. Our working hypothesis is that EBNA2 alters human gene expression by rewiring the chromatin landscape. To test this hypothesis, RNA-seq, ChIP-seq, ATAC-seq, and HiChIP-seq experiments were performed in uninfected, EBV^{EBNA2-} -infected, and EBV^{EBNA2+}-infected Ramos B cells.

Results

EBNA2 modulates human gene expression in EBV-infected B cells

To globally measure the effect of EBNA2 on human gene expression patterns, we performed RNA-seq in Ramos B cells in three experimental conditions – uninfected, EBV^{EBNA2-}, and EBV^{EBNA2+} (Fig. 1). We first examined the presence and absence of EBV-encoded molecules such as EBNA2

and the Epstein–Barr virus-encoded small RNAs (EBERs) across the three cell types. As expected, we only detected transcripts for EBERs in the EBV infected Ramos cells (both EBV^{EBNA2+} and EBV^{EBNA2-}), and we only detected EBNA2 transcripts and protein in EBV^{EBNA2+} cells (Supplemental Fig. S1). Further, no RNA-seq reads mapped to the EBV genome in the uninfected dataset, whereas 7535/7764 and 4249/4423 reads mapped for EBV^{EBNA2+} replicate 1/replicate 2 and EBV^{EBNA2-} replicate 1/replicate 2, respectively.

To investigate the effect of EBNA2 on host gene expression, we identified differentially expressed genes (DEGs) using these three experimental conditions. First, we compared gene expression changes between EBV^{EBNA2+} and uninfected, which captures the effect of EBV infection on human gene expression in B cells. In total, 493 human genes were differentially expressed upon EBV^{EBNA2+} infection (Supplemental Table S1), with 290 genes up-regulated and 203 down-regulated (1.5-fold change or more, adjusted p-value<0.05). Among these 493 EBV-dependent differentially expressed genes, 123 have been reported previously as EBV-dependent in B cells (Wang et al. 2019) (p-value: $1.47E^{-13}$, hypergeometric test).

Next, we identified the EBNA2-specific effects of these gene expression changes. To this end, we identified significant changes in gene expression (1.5-fold change or more, adjusted p-value<0.05) between EBV^{EBNA2+} and uninfected cells, and between EBV^{EBNA2-} and uninfected cells (Figs. 2A and 2B, Supplemental Fig. S2A and S2B, Supplemental Table S1). This procedure identified 421 genes that are differentially expressed in the EBV^{EBNA2+} condition but not in the EBV^{EBNA2-} condition (243 up-regulated genes and 178 down-regulated genes, Supplemental Table S1), which we designate the EBNA2 DEGs. As expected, GO Biological Process enrichment analysis for

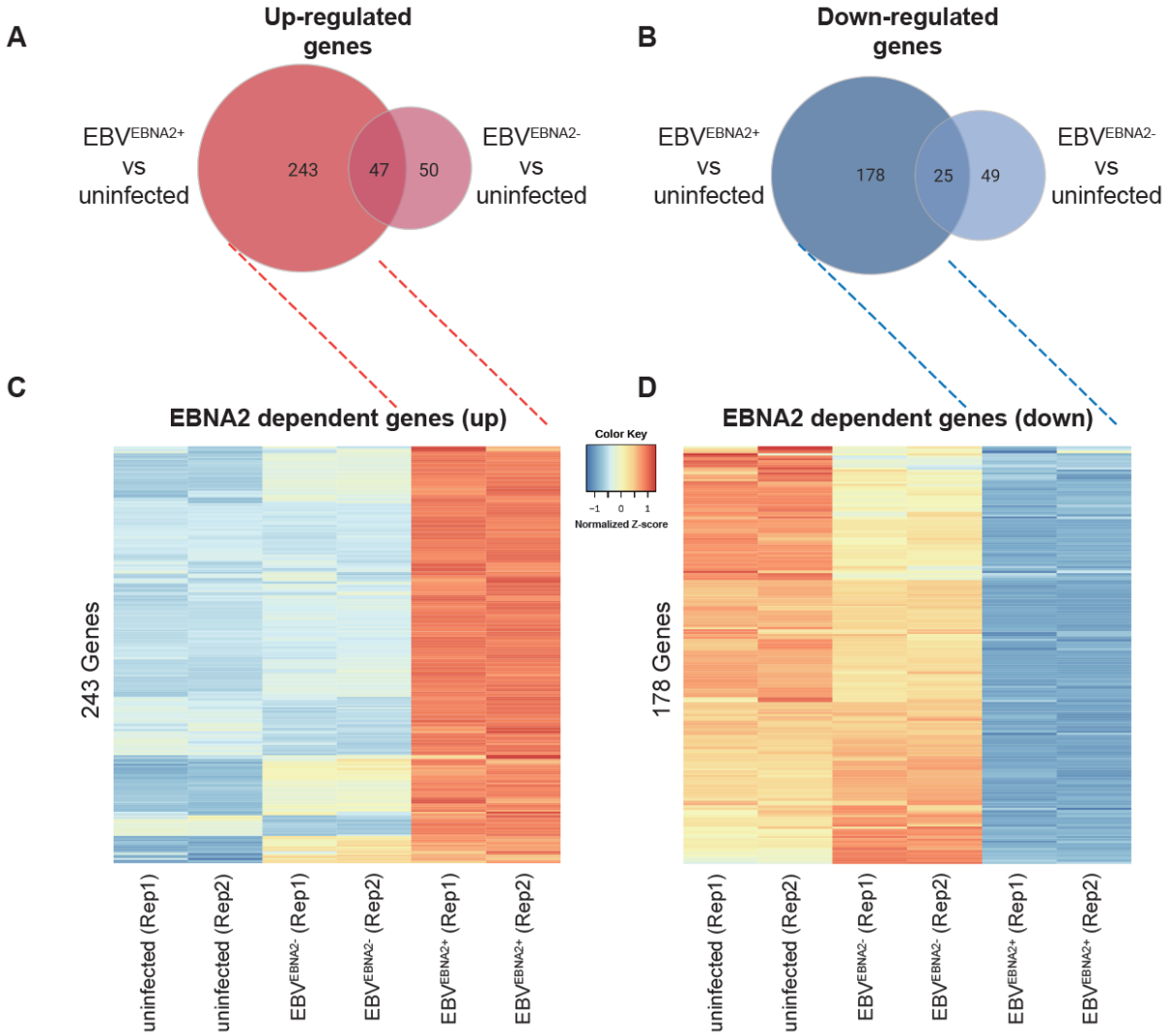

Figure 2. Differential gene expression in EBV-infected Ramos cells. Venn diagrams depicting the number of up-regulated genes (A) and down-regulated genes (B) based on comparisons between EBV^{EBNA2+} vs uninfected and EBV^{EBNA2-} vs uninfected conditions, respectively. Heatmaps indicate genes that are differentially expressed only in EBV^{EBNA2+} conditions.

EBNA2 DEGs revealed processes involved in the immune response, including response to virus, lymphocyte activation, and cytokine production (Supplemental Fig. S3, Supplemental Table S2).

Further, a significant proportion of the EBNA2 DEGs, including *CD80*, *MAP3K8*, *SLAMF1*, and *ZMIZ1*, are involved in leukocyte cell-cell adhesion (adjusted *p*-value: $6.03E^{-3}$, Supplemental Table S2). Collectively, these results indicate that the expression levels of hundreds of human genes are affected by the presence of EBNA2.

EBNA2 occupies regions of the human genome proximal to genes with EBNA2-dependent expression levels

We next performed ChIP-seq for EBNA2 in EBV^{EBNA2+} Ramos cells, identifying 4,219 regions of the genome occupied by EBNA2 (see Methods). We also performed ChIP-seq for EBNA2 in GM12878 cells with high depth sequencing (500 million reads). Comparison of the genomic coordinates of our EBNA2 ChIP-seq datasets to published EBNA2 ChIP-seq datasets using our RELI algorithm (Harley et al. 2018) revealed highly significant concordance (Supplemental Table S3). Likewise, our EBV^{EBNA2+} and GM12878 ChIP-seq peaks aligned significantly with published ChIP-seq peaks of established EBNA2 partners and co-regulators performed in EBV-infected B cells (Zhou et al. 2015), including RBPJ, NFKB1, EBF1, and SPI1 (PU.1) (Supplemental Table S3). As expected, we also observed enrichment within our EBNA2 peaks for the DNA binding motifs of established EBNA2 partners, such as RBPJ, EBF1, and SPI1 (PU.1), as well as chromatin looping factors such as CTCF and YY1 (Supplemental Table S4). Collectively, these results indicate that our EBNA2 ChIP-seq experiments are of high quality.

Next, we investigated the relationship between EBNA2 binding and gene expression changes in Ramos cells using RELI. As expected, EBV^{EBNA2+} Ramos ChIP-seq peaks were enriched within both proximal (promoter, up to 5kb from the transcription start site: 2.4-fold enrichment, adjusted

p-value: $6.52E^{-6}$) and distal (enhancer, up to 100kb from the transcription start site: 1.6-fold enrichment, adjusted *p*-value: $1.77E^{-7}$) regions of EBNA2 DEGs. For example, EBNA2 ChIP-seq peaks are located in the promoter region of EBNA2 DEG *LY9* (Supplemental Fig. S4), in agreement with a recently published finding that *LY9* gene expression is induced by EBV infection (Wang et al. 2019). LY9 protein expression levels have also been shown to be increased in the presence of SLE immune complexes (Hagberg et al. 2013), suggesting a possible role for EBNA2 in *LY9* gene regulation in lupus.

EBNA2 alters chromatin accessibility at hundreds of human genomic loci

We next used our Ramos experimental system to examine the impact of EBNA2 on genome-wide chromatin accessibility by performing ATAC-seq in uninfected, EBV^{EBNA2-}, and EBV^{EBNA2+} conditions (see Methods). In total, we identified 25,931, 12,738, and 30,006 ATAC-seq peaks in these three conditions, respectively. These genomic regions corresponded strongly with previously published datasets performed in relevant cell types, including DNase-seq and ChIP-seq peaks for H3K27ac histone marks (Supplemental Table S5). We examined the impact of EBNA2 on chromatin accessibility by performing differential analysis using MAnorm (Shao et al. 2012) (see Methods), identifying 2,051 and 1,077 EBNA2-dependent open and closed chromatin regions, respectively. For example, we found highly EBNA2-dependent open chromatin in the promoter region of *NAALADL2-AS2*, an uncharacterized antisense long non-coding RNA that is the most highly up-regulated EBNA2 DEG (Fig. 3A).

We next tested the hypothesis that EBNA2 up-regulates genes by opening chromatin and down-regulates genes by closing chromatin. We used RELI to examine the significance of the

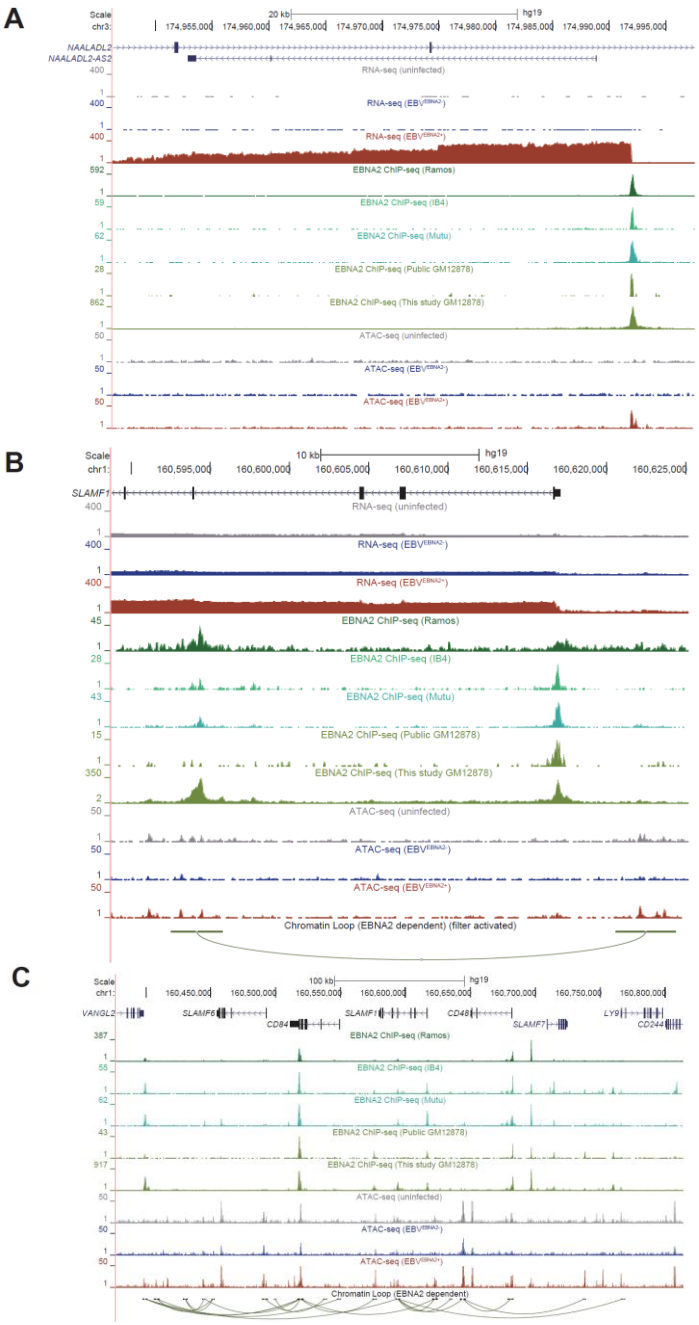

Figure 3. EBNA2-dependent alteration of the human chromatin landscape. (*A*) EBNA2-dependent chromatin opening at the promoter of the upregulated EBNA2 DEG *NAALADL2-AS2*. UCSC Genome Browser screenshot (hg19) depicting binding of EBNA2 within the promoter region of *NAALADL2-AS2*, the most upregulated EBNA2 DEG. (*B*,*C*) EBNA2-dependent alteration of chromatin looping at the *SLAMF1* locus. (*B*) EBNA2-dependent looping to the promoter of the EBNA2 DEG *SLAMF1*. Loops outside of the window are not shown. (*C*) Extensive EBNA2-dependent rewiring of the chromatin looping landscape at the *SLAMF1* locus.

intersection of EBNA2 ChIP-seq peaks, EBNA2-dependent ATAC-seq peaks, and genomic loci harboring EBNA2 DEGs. As expected, these analyses revealed that EBNA2-dependent open chromatin regions tend to fall proximal (within a 5kb window) to upregulated EBNA2 DEGs (5.1-fold enriched, adjusted *p*-value: $2.36E^{-20}$), but not proximal to downregulated EBNA2 DEGs (adjusted *p*-value>0.5). Similar results were obtained for distal (100k window) regions of EBNA2 DEGs (data not shown). Likewise, EBNA2-dependent closed chromatin showed the opposite effect, with enrichment for downregulated EBNA2 DEGs (14.2-fold enriched, adjusted *p*-value: $2.77E^{-65}$) but not upregulated EBNA2 DEGs (adjusted *p*-value>0.5) (Supplemental Table S6). These results collectively reveal an important role for EBNA2 in genome-wide alteration of human chromatin accessibility.

EBNA2 extensively alters the human chromatin looping landscape

Previous reports support a role for EBNA2 in regulating the three-dimensional structure of chromatin looping (Zhao et al. 2011; McClellan et al. 2013; Jiang et al. 2017). Yet, EBNA2's roles in human chromatin looping have not been examined genome-wide. Our integrative analysis of EBNA2 DEGs, EBNA2 ChIP-seq peaks, and EBNA2-specific ATAC-seq peaks revealed significant enrichment at these loci for chromatin looping factors such as CTCF, RAD21, and YY1 (Supplemental Table S3), further supporting a possible role for EBNA2 in chromatin looping alteration. To further elucidate the impact of EBNA2 on chromatin looping across the human genome, we next performed HiChIP-seq with an antibody against H3K27ac in the uninfected, EBV^{EBNA2-}, and EBV^{EBNA2+} conditions (see Methods).

Analysis of the HiChIP-seq data revealed 93,354, 131,296, and 136,689 chromatin looping interactions in the three conditions, respectively. As expected, EBV^{EBNA2+} looping interactions significantly align (3.78-fold enrichment, *p*-value: $4.08E^{-93}$, see Methods) with data from a previously published Hi-C experiment performed in GM12878 cells (Rao et al. 2014). Furthermore, most of the EBV^{EBNA2+} HiChIP-seq peaks coincide with open chromatin regions, as expected (7.1-fold enrichment, adjusted *p*-value $<1E^{-300}$ - 74% of HiChIP-seq peaks have open chromatin on either side in EBV^{EBNA2+} cells). Also as expected, ChIP-seq peaks obtained from relevant cell types for POL2RA and chromatin looping factors such as CTCF, RAD21, and YY1 significantly intersected with HiChIP-seq loop anchors, along with active chromatin marks such as H3K27ac and DNase peaks (Supplemental Table S7). Collectively, these results indicate that our HiChIP-seq data are of high quality.

We next used the HiChIP-seq data to identify EBNA2-dependent differential chromatin looping events (see Methods), identifying 1,972 and 311 looping events that are significantly stronger or weaker in the presence of EBNA2, respectively. As expected, EBNA2-dependent "loop gains" significantly intersect with the promoters of upregulated EBNA2 DEGs, but not the promoters of downregulated EBNA2 DEGs. Likewise, EBNA2-dependent "loop losses" significantly intersect with downregulated EBNA2 DEGs, but not upregulated DEGs (Supplemental Table S8). These findings support a model where EBNA2-induced promoter interactions increase gene expression levels, while EBNA2-induced loss of promoter interactions decreases gene expression levels. In total, 76 newly formed EBNA2-dependent loops fall within the promoters of 57 EBNA2 DEGs (Supplemental Table S6). For example, EBNA2 binds within the *SLAMF1* gene body, resulting in an EBNA2-dependent loop to the promoter of *SLAMF1*, which is one of the most strongly up-

regulated EBNA2-dependent genes (Fig. 3B). Remarkably, the *SLAMF1* locus contains dozens of robust EBNA2-dependent looping events involving multiple genes (Fig. 3C), revealing extensive, EBNA2-dependent rewiring of the chromatin three-dimensional landscape at this locus.

EBNA2-dependent mechanisms significantly coincide with autoimmune disease risk loci

Previous studies (Ricigliano et al. 2015; Harley et al. 2018) have nominated an important role for EBNA2 in autoimmune and other human diseases. We therefore systematically compared the genomic locations of EBNA2-dependent mechanisms to the locations of genetic risk variants obtained from 172 published GWAS datasets (see Methods). Strikingly, the genomic regions surrounding EBNA2 DEGs were enriched for many of the same autoimmune diseases we previously identified based on intersection of GWAS signal with EBNA2 ChIP-seq peaks (Harley et al. 2018). Specifically, 65 of the 421 EBNA2 DEGs (39 up-regulated, 26 down-regulated) have GWAS signal for autoimmune disorders within 100 kilobases of their transcription start site (Fig. 4A, Supplemental Table S9). Among these, 20 and 19 EBNA2 DEGs are located within SLE and MS-associated loci, respectively. In contrast, Non-EBNA2 EBV DEGs do not coincide with autoimmune disease risk loci (Supplemental Table S9), suggesting an EBNA2-specific (as opposed to EBV-specific) role in autoimmune gene regulatory mechanisms.

Next, we inspected EBNA2-dependent chromatin accessibility regions for disease enrichment. Surprisingly, despite the vast changes in chromatin accessibility orchestrated by EBNA2, we did not identify significant intersection between EBNA2-dependent chromatin opening events and autoimmune-associated variants (Fig. 4B, Supplemental Table S9). Rather, we observed enrichment for autoimmune variants within EBNA2-dependent chromatin closing events (4.73-

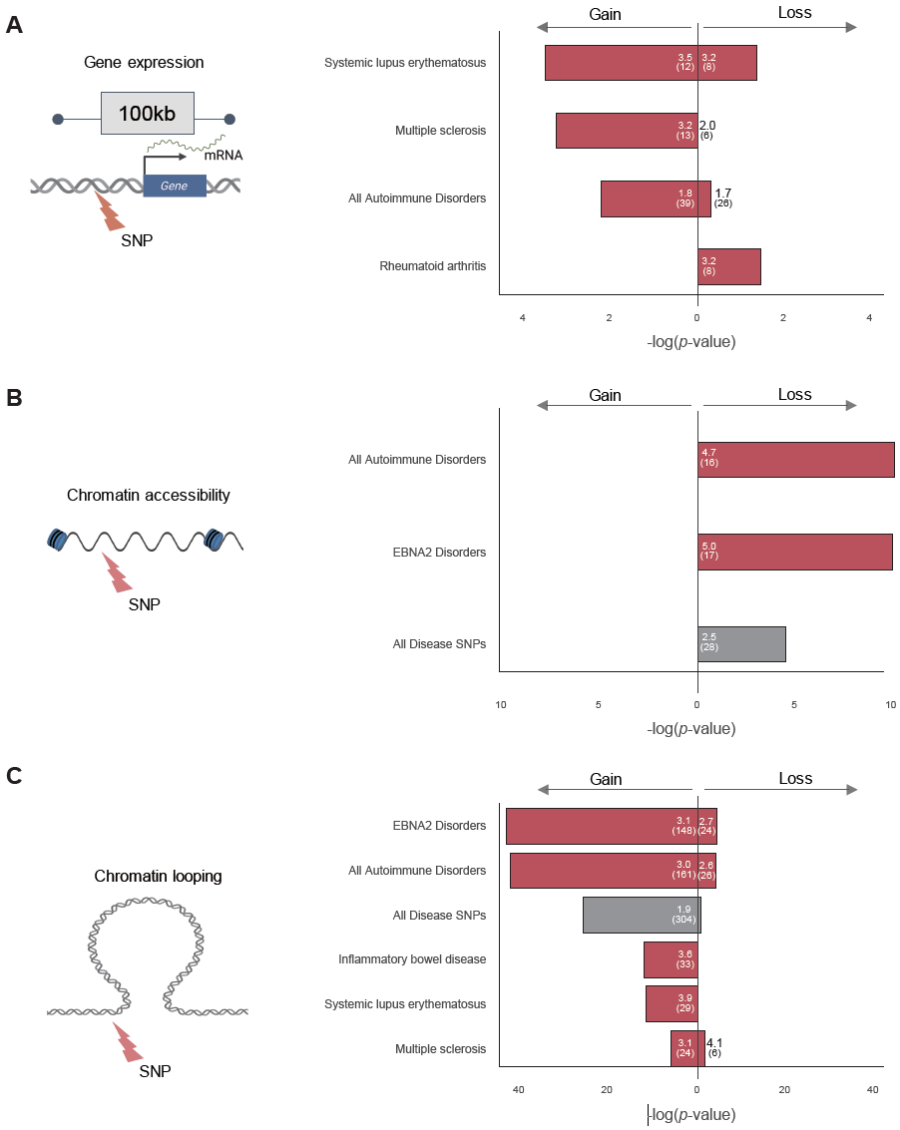

Figure 4. Intersection of EBNA2-dependent gene regulatory mechanisms and disease-associated genetic variants. The bar plot indicates the significance of the intersection (RELI negative $\log_{10}$ adjusted *p*-value). For all analyses, 176 diseases and phenotypes were tested. Only diseases with at least one significant result (3 or more overlaps, corrected *p*-value < 0.05) are shown. Autoimmune diseases are indicated with red bars. Fold-enrichment and number of overlaps are indicated inside the bars. (*A*) Significant intersection between EBNA2-dependent differentially expressed genes and disease-associated variants ('Gain': upregulated genes; 'Loss': downregulated genes, relative to uninfected). (B) Significant intersection between EBNA2-dependent chromatin accessibility and disease-associated variants ('Gain': newly opened chromatin; 'Loss': newly closed chromatin, relative to uninfected). (C) Significant intersection between EBNA2-dependent chromatin looping and disease-associated variants ('Gain': new looping events; 'Loss': loss of looping events, relative to uninfected).

fold enrichment, adjusted *p*-value: $7.69E^{-11}$) (Fig. 4B, Supplemental Table S9). These results prompted us to further examine the relationship between chromatin accessibility and autoimmune risk loci. To this end, we examined the significance of the intersection between autoimmune associated variants and several types of ATAC-seq peaks: 1) constitutively open chromatin regions (i.e., peaks shared in uninfected, EBV^{EBNA2+}, and EBV^{EBNA2-} conditions); 2) EBV-dependent peaks (gains and losses); 3) EBV^{EBNA2-}-dependent peaks (gains and losses); and 4) EBV^{EBNA2+}-dependent peaks (gains and losses). These analyses revealed significant intersection between autoimmune variants and regions of the genome that are constitutively open in B cells (Supplemental Table S10). These results indicate that autoimmune risk variants also concentrate in regions of the genome that are already accessible for the binding of EBNA2 and other proteins prior to infection. Collectively, these analyses reveal that EBNA2-dependent opening of chromatin is not a significant component of autoimmune risk loci; however, EBNA2-dependent chromatin closing, and accessible chromatin prior to EBV infection, are.

Finally, we investigated the relationship between EBNA2-altered chromatin looping interactions and autoimmune disease risk loci. This analysis revealed highly significant intersection between EBNA2-induced changes to chromatin looping and autoimmune disease risk loci. In particular, 161 newly established EBNA2-dependent chromatin loop anchors intersect a total of 547 autoimmune-associated variants (2.98-fold enrichment; adjusted *p*-value: $3.68E^{-43}$) (Fig. 4C, Supplemental Table S9). EBNA2-dependent loss of chromatin looping also shows significant intersection with autoimmune variants, albeit to a much lesser degree (Fig. 4C, Supplemental Table S9). Collectively, these data indicate that EBNA2-dependent alteration of long-range

chromatin interactions is highly associated with autoimmune disease-associated genetic variants, revealing a key role for EBNA2-altered chromatin interactions in autoimmune disease etiology.

Allele-dependent EBNA2 mechanisms at autoimmune-disease risk loci

The previous analyses revealed that EBNA2-dependent chromatin alterations are significantly enriched for autoimmune-associated genetic variants. We therefore next used our MARIO pipeline (Harley et al. 2018) to systematically identify autoimmune risk allele-dependent EBNA2 binding events that coincide with these EBNA2-dependent mechanisms (see Methods). In brief, MARIO identifies genotype-dependent (allelic) functional genomic data (i.e. read imbalance) at genomic locations where the assayed cell contains both the reference and non-reference alleles (i.e., the genotype of the cell must be heterozygous for that specific polymorphism).

Using this approach, we discovered 18 instances of allele-dependent EBNA2 binding at autoimmune risk variants (6 in EBV^{EBNA2+} Ramos, and 12 in GM12878 cells) (Supplemental Table S11). For example, we identified strong EBNA2 allele-dependent binding in EBV^{EBNA2+} Ramos cells to an MS-associated variant (rs1250567) located in the *ZMIZ1* locus (Fig 5A). This region loops to the promoter of the short isoform of *ZMIZ1* in EBV^{EBNA2+} Ramos cells. *ZMIZ1* expression levels are three-fold lower in EBV^{EBNA2+} Ramos cells compared to uninfected Ramos cells, consistent with a previous report by Fewing et al. describing decreased ZMIZ1 protein expression in MS patient blood samples (Fewings et al. 2017). As a second example, we observed strong (>2-fold) allele-dependent EBNA2 binding in GM12878 cells to a vitiligo associated variant (rs867234) located within the promoter of the upregulated EBNA2 DEG *CD80* (Fig. 5B, 8-fold increase in gene expression). Although the variant is not heterozygous in Ramos, IB4, or Mutu

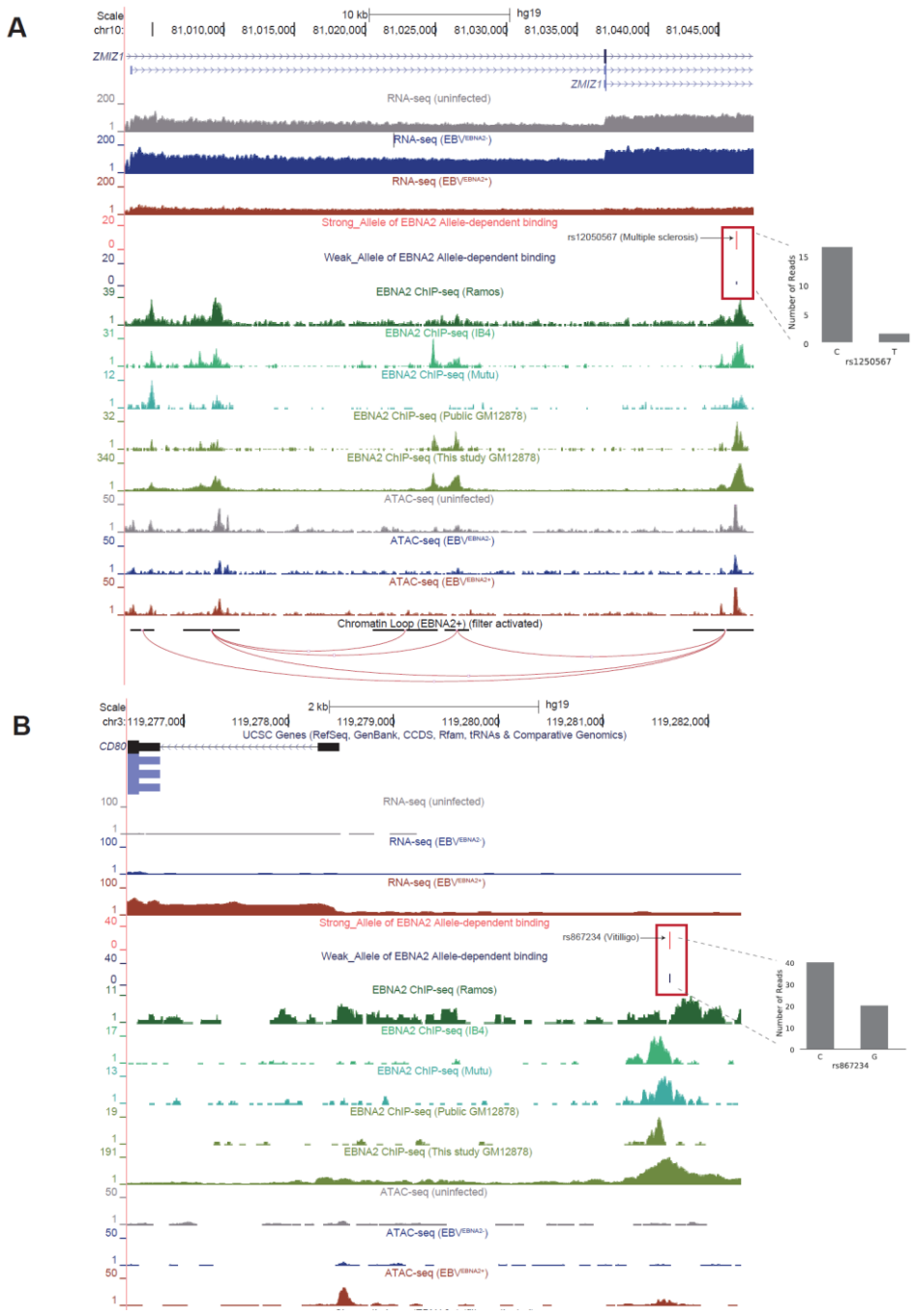

Figure 5. Allele-dependent and EBNA2-dependent mechanisms at autoimmune-associated genetic variants. UCSC Genome Browser shots (hg19) depicting EBNA2-based mechanisms at the *ZMIZ1* (A) and *CD80* (B) loci. Loops outside of the window are not shown (filtered). Red boxes indicate regions where EBNA2 binds in an allele-dependent manner. The ratio of reads between alleles is shown as a bar plot. See text for details.

cells, we also observe binding of EBNA2 in these cells. Together, these examples reveal EBNA2 and autoimmune risk allele-dependent mechanisms possibly underlying the established roles played by genetics and the environment in these complex diseases.

Discussion

In this study, we examined the mechanisms by which an EBV-encoded transcriptional regulator, EBNA2, modulates human gene regulatory programs through genome-wide perturbation of the human chromatin landscape. Our findings show that EBNA2 affects cellular gene regulation using three of the same mechanisms a host regulatory protein might use: 1) interacting with promoters and enhancers; 2) altering chromatin accessibility; and 3) forming new chromatin 3D interactions. We demonstrate that many of these mechanisms significantly intersect autoimmune-associated genetic variants, and identify multiple EBNA2 interactions that are autoimmune risk allele-dependent.

It has been extensively reported that multiple human diseases have a strong EBV-based component (Bray et al. 1983; Serafini et al. 2007; Pender and Burrows 2014) or EBNA2 component (Ricigliano et al. 2015; Harley et al. 2018). In this study, by controlling both EBV infection and the presence of EBNA2 in the EBV-infected cells, we not only corroborate these previous findings, but also identify additional gene targets and mechanisms by which EBV and EBNA2 might affect the course of these diseases. In particular, we observe significant intersection between autoimmune-associated genetic variants and EBNA2-dependent modulation of human gene expression, chromatin accessibility, and chromatin looping interactions (Fig. 4).

Previous studies have demonstrated a key role for EBNA2 in multiple biological processes, including B cell transformation (Saha and Robertson 2019), interferon regulation (Kanda et al. 1992), and NF-kB regulation (Kim et al. 2017). In this study, we find that several genes involved in leukocyte cell-cell adhesion display EBNA2-dependent gene expression levels and regulatory mechanisms, including *NAALADL2-AS2*, *CD80*, *SLAMF1*, and *ZMIZ1*. Importantly, several of these interactions are autoimmune disease risk-allele dependent. EBV infection is known to alter the expression of adhesion molecules and receptors (Zhao et al. 2006; Shannon-Lowe and Rowe 2011; Grossman et al. 2017). In particular, Fewing et al. reported a negative correlation between *ZMIZ1* expression and EBV antigen levels (Fewings et al. 2017), consistent with the EBNA2-dependent decrease in *ZMIZ1* expression that we observe. Further, previous studies have reported elevated expression levels of adhesion molecules in SLE patients (Funauchi et al. 1993; Egerer et al. 2000) and MS patients (Elovaara et al. 2000). Together, these results support a model where EBNA2 affects autoimmune disease onset and/or progression through the alteration of cell-cell adhesion-related gene regulatory programs.

In addition to possible EBNA2 roles in the regulation of cell-cell adhesion genes, we observed widespread EBNA2-dependent chromatin looping events at a genomic locus encoding multiple members of the signaling lymphocyte activation molecule (SLAM) family, including *CD84*, *SLAMF1*, and *LY9*. SLAM family genes were previously reported to have EBV-dependent gene expression patterns (Wang et al. 2019), with *SLAMF1* in particular being among the most strongly up-regulated EBNA2 target genes (Maier et al. 2006). SLAM family genes play key roles in several immunological processes, including humoral responses (Ma et al. 2007), development and

maintenance of immune system function (Schwartzberg et al. 2009), and cell adhesion (reviewed in (Cannons et al. 2011)). Our new results establish a possible role for EBNA2 in the regulation of the SLAM-mediated autoimmune-related immune response.

A limitation of our study design is that P3HR1 and B95.8 are different genetic isolates of EBV. Therefore, there are further genetic differences between the isolates in addition to the EBNA2 deletion. For example, the last two exons (45 amino acids) of EBNA-LP are also deleted in the P3HR1 virus. However, EBV mutants with these two exons deleted can still transform primary B cells, albeit at lower frequencies (Mannick et al. 1991). Further, P3HR1 is a well-established model system that has been widely used as an EBNA2-null strain in the field of virology for decades (Murray et al. 1988; Zimber-Strobl et al. 1991; Lee et al. 2002; Jiang et al. 2017).

In summary, our findings reveal an important role for the EBV-encoded EBNA2 regulatory protein in multiple mechanisms that ultimately affect human gene expression levels. Several of these mechanisms are allele-dependent at variants associated with autoimmune diseases such as MS and SLE. It is possible that other viral transcriptional regulators play similar mechanistic roles in other diseases. Future studies will deepen our knowledge of the mechanisms underlying virus-host interactions, and ultimately provide both a rationale and a foundation for therapeutic approaches targeting these interactions.

Methods

EBV infection of Ramos B cells

Wild-type B95.8 EBV (EBV^{EBNA2+}) and P3HR1 EBV lacking EBNA2 (EBV^{EBNA2-}) were prepared from B95.8 and P3HR1 cell supernatants respectively, and cultured in 10% FBS supplemented RPMI medium 1640 for 2 weeks. Viral suspension was filtered via 0.45 μm Millipore filters and cells were pelleted. The concentrated viral stocks were stored at –80 °C. Ramos cells (EBV Negative, ATCC CRL-1596) were infected ~2 x 10^6/ml with viral stock based on infection optimization assays and incubated for 4 hours for virus adsorption. After infection, cells were washed and cultured. After 10 passages, we confirmed the infection by morphological changes and the expression of EBNA2 viral protein levels as previously published (Harley et al. 2018).

RNA-seq

Total RNA was extracted using the mirVANA Isolation Kit (Ambion) from Ramos B cells in each of the three conditions: uninfected Ramos (uninfected), EBNA2-positive EBV (B95.8)-infected Ramos (EBV^{EBNA2+}), and EBNA2-negative EBV (P3HR1)-infected Ramos (EBV^{EBNA2-}). RNA was extracted at the same time point for every condition. RNA was depleted of ribosomal RNA using the Ribo-Zero rRNA removal kit and sequenced at Cincinnati Children's Hospital Medical Center (CCHMC) DNA Sequencing and Genotyping Core Facility. Using the tool FastQC (version: 0.11.2) (http://www.bioinformatics.babraham.ac.uk/projects/fastqc), all data were confirmed to pass all quality control checks, except for adapter sequence contents, which were removed using cutadapt (trimgalore version: 0.4.2)(https://journal.embnet.org/index.php/embnetjournal/article/view/200). RNA-seq reads were aligned to the hg19 (GrCh37) genome build (NCBI) using Spliced Transcripts Alignment to a Reference (STAR, version: 020201) (https://doi.org/10.1093/bioinformatics/bts635). The featureCounts function (Rsubread version: 3.5.3) was used to count reads (Liao et al. 2014) and

DESeq2 (version 3.5.3) was used to perform differential gene expression (Love et al. 2014). DESeq2 results were filtered to only include genes with fragments per kilobase per million (FPKM) values greater than one in at least one condition. Differential expression was calculated with thresholds of a greater than 1.5-fold change and an adjusted *p*-value threshold of less than 0.05 (*p*-values were adjusted by Benjamini and Hochberg false discovery rate (FDR)). Gene set enrichment analysis was performed using ToppFun (Chen et al. 2009).

ChIP-seq

Ramos and GM12878 cells were crosslinked and nuclei were sonicated as described previously (Lu et al. 2015). Cells were incubated in crosslinking solution (1% formaldehyde, 5 mM HEPES [pH 8.0], 10 mM sodium chloride, 0.1 mM EDTA, and 0.05 mM EGTA in RPMI medium 1640 with 10% FBS) and placed on a tube rotator at room temperature for 10 min. To stop the crosslinking, glycine was added to a final concentration of 0.125 M and tubes were placed back on the rotator at room temperature for 5 min. Cells were washed twice with ice-cold PBS, resuspended in lysis buffer 1 (50 mM HEPES [pH 7.5], 140 mM NaCl, 1 mM EDTA, 10% glycerol, 0.25% Triton X-100, and 0.5% NP-40), and incubated for 10 min on ice. Nuclei were harvested after centrifugation at 5,000 rpm for 10 min, resuspended in lysis buffer 2 (10 mM Tris-HCl [pH 8.0], 1 mM EDTA, 200 mM NaCl, and 0.5 mM EGTA), and incubated at room temperature for 10 min. Protease and phosphatase inhibitors were added to both lysis buffers. Nuclei were then resuspended in sonication buffer (10 mM Tris [pH 8.0], 1 mM EDTA, and 0.1% SDS). A S220 focused ultrasonicator (COVARIS) was used to shear chromatin (150- to 500-bp fragments) with 10% duty cycle, 175 peak power, and 200 bursts per cycle for 7 min. A portion of

the sonicated chromatin was run on an agarose gel to verify fragment sizes. Sheared chromatin was precleared with 20 µl Dynabeads Protein G (Life Technologies) at 4 °C for 40 min.

Immunoprecipitation of EBNA2-chromatin complexes was performed with an SX-8X IP-STAR compact automated system (Diagenode). Beads conjugated to antibodies against EBNA2 (Abcam; ab90543) were incubated with precleared chromatin at 4°C for 8 hours. The beads were then washed sequentially with wash buffer 1 (10 mM Tris-HCl [pH 7.5], 150 mM NaCl, 1 mM EDTA, 0.1% SDS, 0.1% NaDOC, and 1% Triton X-100), wash buffer 2 (10 mM Tris-HCl [pH 7.6], 400 mM NaCl, 1 mM EDTA, 0.1% SDS, 0.1% NaDOC, and 1% Triton X-100), wash buffer 3 (10 mM Tris-HCl [pH 8.0], 250 mM LiCl, 1 mM EDTA, 0.5% NaDOC, and 0.5% NP-40), and wash buffer 4 (10 mM Tris-HCl [pH 8.0], 1 mM EDTA, and 0.2% Triton X-100). Finally, the beads were resuspended in 10 mM Tris-HCl (pH 7.5) and used to prepare libraries via ChIPmentation (Schmidl et al. 2015).

We performed quality control of raw sequencing reads using FastQC (version: 0.11.2) (http://www.bioinformatics.babraham.ac.uk/projects/fastqc). All data were confirmed to pass all quality control checks, except for adapter sequence contents, which were removed using cutadapt (trimgalore version: 0.4.2). For EBNA2 ChIP-seq in Ramos cells, paired-end fastq files were used for peak calling. Alignment of reads to the human genome (build hg19) was performed using Bowtie2 (Langmead and Salzberg 2012). For GM12878, we merged 16 single-end BAM files and 5 paired-ended BAM files from individual experiments for peak calling. Peaks were called using Model-based Analysis of ChIP-Seq version 2.1.1 (MACS2) (Feng et al. 2012) with the following arguments: -g hs -q 0.01 --broad. These settings were chosen from several tested parameter

combinations because they yielded the best TF binding site motif enrichment p-values (using HOMER) for EBNA2 binding partner RBPJ. Differential binding of EBNA2 compared to input was calculated using MAnorm (Shao et al. 2012) with a threshold of 1.5 or greater fold change and a *p*-value of less than 0.05. For comparison, we also obtained publicly available EBNA2 ChIP-seq datasets (GM12878 cells: SRR3101734; IB4 cells: SRR332245; Mutu cells: SRR8783824), and called peaks using MACS2 with the following arguments: -g hs -q 0.01.

ATAC-seq

ATAC-seq was performed in the three Ramos cell conditions. Briefly, transposase Tn5 with adapter sequences was used to cut accessible DNA. These accessible DNA with adaptor sequences were isolated, then libraries were prepared for uninfected, EBV^{EBNA2-}, EBV^{EBNA+} Ramos using a standard protocol (Buenrostro et al. 2015). Sequencing was performed at the CCHMC DNA Sequencing and Genotyping Core Facility. FastQC was used to perform quality control (http://www.bioinformatics.babraham.ac.uk/projects/fastqc), as described above. Before alignment, all replicates that passed FastQC were pooled within each condition (Passed replicate number: 6 for uninfected, 5 for EBV^{EBNA2-}, and 6 for EBV^{EBNA2+})

ATAC-seq reads were aligned to the human genome (hg19) using Bowtie2 (Langmead and Salzberg 2012) and peaks were called using MACS2 (same version as ChIP-seq) (Feng et al. 2012). Differential chromatin accessibility was calculated using the MAnorm program (Shao et al. 2012) and bedtools (Quinlan and Hall 2010). First, we determined EBV-dependent open chromatin by calculating B958-unique peaks compared to uninfected peaks (>1.5 fold, p-value < 0.05) using MAnorm. Next, to obtain EBNA2-dependent regions, we subtracted EBV^{EBNA2-}-unique peaks

compared to uninfected using the bedtools subtract command. To identify EBNA2-dependent closed chromatin, we first determined EBV-dependent closed chromatin, by identifying uninfected-unique peaks compared to EBV^{EBNA2+} peaks, then intersected these with EBV^{EBNA2-}-unique peaks compared to EBV^{EBNA2+} peaks.

HiChIP-seq

HiChIP-seq libraries were prepared following Mumbach *et al.* (Mumbach et al. 2016). Cells were cross-linked with 1% formaldehyde and lysed with Hi-C lysis buffer. Cross-linked DNA was digested by MboI. DNA ends were filled with biotin-dATP and dCTP, dTTP, dGTP and then ligated by T4 DNA ligase. After ligation, DNA was sonicated using a Covaris M220. Fragmented DNA was then diluted 10 times with ChIP dilution buffer and protein-DNA complexes were captured using an H3K27ac antibody (Abcam AB4729). Next, protein-DNA complexes were further captured by protein A beads and eluted. DNA was purified after reverse crosslinking. Biotin dATP-labeled DNA was captured with Streptavidin C-1 beads and PCR amplified using Phusion HF (New England Biosciences) and 1 μL of each Nextera forward primer (Ad1_noMX) and Nextera reverse primer (Ad2.X). The libraries were sequenced using Illumina Nextseq (2x75bp).

We used HiC-pro (version: 2.11.0) to align reads and identify the Hi-C contact map (Servant et al. 2015). We then integrated the aligned Hi-C data with the ChIP-seq data to correct the background, perform restriction site bias modeling and obtain looping information using hichipper (version: 0.7.3) (http://aryeelab.org/hichipper). We identified differential looping events using the diffloop Bioconductor R package (1.6.0) (Lareau and Aryee 2018). Briefly, to calculate EBNA2-dependent

differential looping, we first determined EBV-dependent chromatin looping by comparing EBV^{EBNA2+} looping events to uninfected looping events using diffloop (>1.5 fold change, *p*-value < 0.05). Likewise, we also compared EBV^{EBNA2-} looping events to uninfected looping events using the same cutoffs. Then to identify EBNA2-dependent looping events, we applied diffloop again, comparing EBV^{EBNA2+}-dependent looping events to EBV^{EBNA2-}-dependent looping events, using the same cutoffs. We calculated the significance of the intersection between chromatin looping events in EBV^{EBNA2+} conditions using looping data from GM12878 cells (Rao et al. 2014), obtained from The 3D Genome Browser (Wang et al. 2018), using a permutation test. Specifically, we randomized EBV^{EBNA2+} loop coordinates, using 500 iterations of permutation, then calculated a z-score by comparing the distribution of randomized intersection counts to actual intersection counts.

Estimation of the significance of intersected genomic coordinates using RELI

We used the RELI method to calculate the significance of intersection between the genomic coordinates of two or more datasets. In brief, RELI calculates the overlap between the input genomic coordinates and a library of ChIP-seq derived genomic coordinates. It then permutes the input coordinates to calculate the overlap between randomized coordinates and the library coordinates. After 2,000 iterations, RELI then compares the randomized overlap to the actual overlap, and calculates the significance of this overlap (Harley et al. 2018). We used a RELI library containing 1,544 TF datasets, 2,455 Non-TF datasets, and disease-associated genetic variants (through GWAS) from 172 diseases (Harley et al. 2018). Search windows (100 kb for distal, 5kb for promoter) were padded from the transcription start site (TSS) coordinates of EBNA2 DEGs. We ran RELI (null model: OpenChrom) with padded DEGs, EBNA2 ChIP-seq, EBNA2-

dependent chromatin, and EBNA2 looping interactions. RELI output was filtered based on the number of overlaps (greater than 3) and significance (adjusted *p*-value<0.05, Bonferroni correction), following our standard practices.

Identification of allele-dependent sequencing reads using MARIO

Allele-dependent behavior was identified in sequencing reads using the MARIO pipeline (Harley et al. 2018). Briefly, the MARIO pipeline identifies allele-dependent behavior by weighing 1) the imbalance between the number of reads that are mapped to each allele, 2) the total number of reads mapped at each variant, and 3) the number of and the consistency of available replicates. These variables are combined into a single Allelic Reproducibility Score (ARS), which reflects the degree of allelic behavior observed for the given heterozygous variant in the given dataset. To identify heterozygous variants, we used genotyping array data for Ramos cells (Harley et al. 2018) and GM12878 cells (dbGaP ID: phs001989.v1). Imputation was performed using the impute2 program (Howie et al. 2009). MARIO ARS values exceeding 0.4 were considered to be allelic, following our previous study (Harley et al. 2018).

TF DNA binding motif enrichment analysis

We used the HOMER software package (Heinz et al. 2010) to calculate TF DNA binding site motif enrichment. We used a modified version of HOMER that incorporates human motifs obtained from CisBP build 2.0 (Weirauch et al. 2014; Lambert et al. 2019).

GWAS dataset curation

We obtained GWAS data from multiple studies from the NHGRI-EBI GWAS Catalog (version GWAS_catalog_v1.0.2-associations_e96_r2019-05-03) (Buniello et al. 2019). A genome wide significance cutoff of 5×10^{-8} was used to establish the statistical significance of a variant and its association to a given disease or trait. After filtering for genome wide association, variants were grouped based on the disease or trait reported in the publication as well as the reported ancestries. For each disease/trait, independent loci were identified using LD-based pruning in Plink (window size 300,000 kb, SNP shift size 100,000 kb, and $r2 < 0.2$).

Data and code access

USCC Genome Browser session:

http://genome.ucsc.edu/s/hon9dt/EBNA2_Ramos_Chromatin_Paper

GEO accession (RNA-seq, ChIP-seq, ATAC-seq, HiChIP-seq):

GSE148396

dbGAP (genotyping):

phs001989.v1

Published data sets (EBNA2 ChIP-seq):

- GM12878 cells: SRR3101734
- IB4 cells: SRR332245
- Mutu cells: SRR8783824

RELI source code: https://github.com/WeirauchLab/RELI

MARIO source code: https://github.com/WeirauchLab/MARIO

Acknowledgments

The authors thank Artem Barski for maintaining robot facilities for ChIP-seq experiments. The authors thank Kevin Ernst for critical input on technical issues and computational support including servers, software packages, and data management. The authors also thank Mario Pujato (CCHMC Bioinformatics Collaborative Services) and Xiaoting Chen for insights related to data analysis. Finally, the authors acknowledge that the cartoons from Figure 1 and Figure 4 were created using BioRender.com.

Funding sources

This study was supported by NIH grants R01 NS099068 and R01 GM055479 (M.T.W.); R01 AR073228 (L.C.K. and M.T.W.); R01 DK107502 and P30 AR070549 (L.C.K.); and U01 AI130830, U01 HG008666, R01 AI024717, R01 AI148276, and I01 BX001834 (J.B.H.). This study was further supported by funding from the Ohio Supercomputing Center (M.T.W.), along with funds from Cincinnati Children's Research Foundation ARC and CpG awards (M.T.W., L.C.K., and J.B.H.) and a CCRF Endowed Scholar Award (M.T.W.)

References

Agudelo-Romero P, Carbonell P, Perez-Amador MA, Elena SF. 2008. Virus adaptation by manipulation of host's gene expression. *PLoS One* **3**: e2397.

Ascherio A, Munger KL. 2007. Environmental risk factors for multiple sclerosis. Part I: the role of infection. *Ann Neurol* **61**: 288-299.

Bagert BA. 2009. Epstein-Barr virus in multiple sclerosis. *Curr Neurol Neurosci Rep* **9**: 405-410.

Balandraud N, Roudier J. 2018. Epstein-Barr virus and rheumatoid arthritis. *Joint Bone Spine* **85**: 165-170.

Beagan JA, Duong MT, Titus KR, Zhou L, Cao Z, Ma J, Lachanski CV, Gillis DR, Phillips-Cremins JE. 2017. YY1 and CTCF orchestrate a 3D chromatin looping switch during early neural lineage commitment. *Genome Res* **27**: 1139-1152.

Bermudez-Morales VH, Peralta-Zaragoza O, Alcocer-Gonzalez JM, Moreno J, Madrid-Marina V. 2011. IL-10 expression is regulated by HPV E2 protein in cervical cancer cells. *Mol Med Rep* **4**: 369-375.

Bochkov YA, Hanson KM, Keles S, Brockman-Schneider RA, Jarjour NN, Gern JE. 2010. Rhinovirus-induced modulation of gene expression in bronchial epithelial cells from subjects with asthma. *Mucosal Immunol* **3**: 69-80.

Bookman EB, McAllister K, Gillanders E, Wanke K, Balshaw D, Rutter J, Reedy J, Shaughnessy D, Agurs-Collins T, Paltoo D et al. 2011. Gene-environment interplay in common complex diseases: forging an integrative model-recommendations from an NIH workshop. *Genetic epidemiology* **35**: 217-225.

Bray PF, Bloomer LC, Salmon VC, Bagley MH, Larsen PD. 1983. Epstein-Barr virus infection and antibody synthesis in patients with multiple sclerosis. *Arch Neurol* **40**: 406-408.

Buenrostro JD, Wu B, Chang HY, Greenleaf WJ. 2015. ATAC-seq: A Method for Assaying Chromatin Accessibility Genome-Wide. *Curr Protoc Mol Biol* **109**: 21 29 21-29.

Buniello A, MacArthur JAL, Cerezo M, Harris LW, Hayhurst J, Malangone C, McMahon A, Morales J, Mountjoy E, Sollis E et al. 2019. The NHGRI-EBI GWAS Catalog of published genome-wide association studies, targeted arrays and summary statistics 2019. *Nucleic Acids Res* **47**: D1005-D1012.

Caliskan M, Baker SW, Gilad Y, Ober C. 2015. Host genetic variation influences gene expression response to rhinovirus infection. *PLoS Genet* **11**: e1005111.

Cannons JL, Tangye SG, Schwartzberg PL. 2011. SLAM family receptors and SAP adaptors in immunity. *Annu Rev Immunol* **29**: 665-705.

Chen J, Bardes EE, Aronow BJ, Jegga AG. 2009. ToppGene Suite for gene list enrichment analysis and candidate gene prioritization. *Nucleic Acids Res* **37**: W305-311.

Clyde K, Glaunsinger BA. 2010. Getting the message direct manipulation of host mRNA accumulation during gammaherpesvirus lytic infection. *Adv Virus Res* **78**: 1-42.

Deplancke B, Alpern D, Gardeux V. 2016. The Genetics of Transcription Factor DNA Binding Variation. *Cell* **166**: 538-554.

Dimitroulia E, Pitiriga VC, Piperaki ET, Spanakis NE, Tsakris A. 2013. Inflammatory bowel disease exacerbation associated with Epstein-Barr virus infection. *Dis Colon Rectum* **56**: 322-327.

Dunmire SK, Hogquist KA, Balfour HH. 2015. Infectious Mononucleosis. *Curr Top Microbiol Immunol* **390**: 211-240.

Egerer K, Feist E, Rohr U, Pruss A, Burmester GR, Dorner T. 2000. Increased serum soluble CD14, ICAM-1 and E-selectin correlate with disease activity and prognosis in systemic lupus erythematosus. *Lupus* **9**: 614-621.

Elovaara I, Ukkonen M, Leppakynnas M, Lehtimaki T, Luomala M, Peltola J, Dastidar P. 2000. Adhesion molecules in multiple sclerosis: relation to subtypes of disease and methylprednisolone therapy. *Arch Neurol* **57**: 546-551.

Feng J, Liu T, Qin B, Zhang Y, Liu XS. 2012. Identifying ChIP-seq enrichment using MACS. *Nat Protoc* **7**: 1728-1740.

Fewings NL, Gatt PN, McKay FC, Parnell GP, Schibeci SD, Edwards J, Basuki MA, Goldinger A, Fabis-Pedrini MJ, Kermode AG et al. 2017. The autoimmune risk gene ZMIZ1 is a vitamin D responsive marker of a molecular phenotype of multiple sclerosis. *J Autoimmun* **78**: 57-69.

Flavahan WA, Gaskell E, Bernstein BE. 2017. Epigenetic plasticity and the hallmarks of cancer. *Science* **357**.

Flemington E, Speck SH. 1990. Epstein-Barr virus BZLF1 trans activator induces the promoter of a cellular cognate gene, c-fos. *J Virol* **64**: 4549-4552.

Foxman EF, Iwasaki A. 2011. Genome-virome interactions: examining the role of common viral infections in complex disease. *Nat Rev Microbiol* **9**: 254-264.

Funauchi M, Ohno M, Minoda M, Horiuchi A. 1993. Abnormal expression of intercellular adhesion molecule-1 on peripheral blood mononuclear cells from patients with systemic lupus erythematosus. *J Clin Lab Immunol* **40**: 115-124.

Graham SV. 2016. Human Papillomavirus E2 Protein: Linking Replication, Transcription, and RNA Processing. *J Virol* **90**: 8384-8388.

Grossman L, Chang C, Dai J, Nikitin PA, Jima DD, Dave SS, Luftig MA. 2017. Epstein-Barr Virus Induces Adhesion Receptor CD226 (DNAM-1) Expression during Primary B-Cell Transformation into Lymphoblastoid Cell Lines. *mSphere* **2**.

Hagberg N, Theorell J, Schlums H, Eloranta ML, Bryceson YT, Ronnblom L. 2013. Systemic lupus erythematosus immune complexes increase the expression of SLAM family members CD319 (CRACC) and CD229 (LY-9) on plasmacytoid dendritic cells and CD319 on CD56(dim) NK cells. *J Immunol* **191**: 2989-2998.

Harley JB, Chen X, Pujato M, Miller D, Maddox A, Forney C, Magnusen AF, Lynch A, Chetal K, Yukawa M et al. 2018. Transcription factors operate across disease loci, with EBNA2 implicated in autoimmunity. *Nat Genet* **50**: 699-707.

Harley JB, James JA. 2006. Epstein-Barr virus infection induces lupus autoimmunity. *Bull NYU Hosp Jt Dis* **64**: 45-50.

Heinz S, Benner C, Spann N, Bertolino E, Lin YC, Laslo P, Cheng JX, Murre C, Singh H, Glass CK. 2010. Simple combinations of lineage-determining transcription factors prime cis-regulatory elements required for macrophage and B cell identities. *Mol Cell* **38**: 576-589.

Henkel T, Ling PD, Hayward SD, Peterson MG. 1994. Mediation of Epstein-Barr virus EBNA2 transactivation by recombination signal-binding protein J kappa. *Science* **265**: 92-95.

Hindorff LA, Sethupathy P, Junkins HA, Ramos EM, Mehta JP, Collins FS, Manolio TA. 2009. Potential etiologic and functional implications of genome-wide association loci for human diseases and traits. *Proc Natl Acad Sci U S A* **106**: 9362-9367.

Hong JY, Bentley JK, Chung Y, Lei J, Steenrod JM, Chen Q, Sajjan US, Hershenson MB. 2014. Neonatal rhinovirus induces mucous metaplasia and airways hyperresponsiveness through IL-25 and type 2 innate lymphoid cells. *J Allergy Clin Immunol* **134**: 429-439.

Howie BN, Donnelly P, Marchini J. 2009. A flexible and accurate genotype imputation method for the next generation of genome-wide association studies. *PLoS Genet* **5**: e1000529.

Hunter DJ. 2005. Gene-environment interactions in human diseases. *Nat Rev Genet* **6**: 287-298.

Jiang S, Zhou H, Liang J, Gerdt C, Wang C, Ke L, Schmidt SCS, Narita Y, Ma Y, Wang S et al. 2017. The Epstein-Barr Virus Regulome in Lymphoblastoid Cells. *Cell Host Microbe* **22**: 561-573 e564.

Kamen DL. 2014. Environmental influences on systemic lupus erythematosus expression. *Rheum Dis Clin North Am* **40**: 401-412, vii.

Kanda K, Decker T, Aman P, Wahlstrom M, von Gabain A, Kallin B. 1992. The EBNA2-related resistance towards alpha interferon (IFN-alpha) in Burkitt's lymphoma cells effects induction of IFN-induced genes but not the activation of transcription factor ISGF-3. *Mol Cell Biol* **12**: 4930-4936.

Kim JH, Kim WS, Hong JY, Ryu KJ, Kim SJ, Park C. 2017. Epstein-Barr virus EBNA2 directs doxorubicin resistance of B cell lymphoma through CCL3 and CCL4-mediated activation of NF-kappaB and Btk. *Oncotarget* **8**: 5361-5370.

Lambert SA, Jolma A, Campitelli LF, Das PK, Yin Y, Albu M, Chen X, Taipale J, Hughes TR, Weirauch MT. 2018. The Human Transcription Factors. *Cell* **172**: 650-665.

Lambert SA, Yang AWH, Sasse A, Cowley G, Albu M, Caddick MX, Morris QD, Weirauch MT, Hughes TR. 2019. Similarity regression predicts evolution of transcription factor sequence specificity. *Nat Genet* **51**: 981-989.

Langmead B, Salzberg SL. 2012. Fast gapped-read alignment with Bowtie 2. *Nat Methods* **9**: 357-359.

Lareau CA, Aryee MJ. 2018. diffloop: a computational framework for identifying and analyzing differential DNA loops from sequencing data. *Bioinformatics* **34**: 672-674.

Lee JM, Lee KH, Weidner M, Osborne BA, Hayward SD. 2002. Epstein-Barr virus EBNA2 blocks Nur77- mediated apoptosis. *Proc Natl Acad Sci U S A* **99**: 11878-11883.

Lee TI, Young RA. 2013. Transcriptional regulation and its misregulation in disease. *Cell* **152**: 1237-1251.

Liao Y, Smyth GK, Shi W. 2014. featureCounts: an efficient general purpose program for assigning sequence reads to genomic features. *Bioinformatics* **30**: 923-930.

Love MI, Huber W, Anders S. 2014. Moderated estimation of fold change and dispersion for RNA-seq data with DESeq2. *Genome Biol* **15**: 550.

Lu F, Chen HS, Kossenkov AV, DeWispeleare K, Won KJ, Lieberman PM. 2016. EBNA2 Drives Formation of New Chromosome Binding Sites and Target Genes for B-Cell Master Regulatory Transcription Factors RBP-jkappa and EBF1. *PLoS Pathog* **12**: e1005339.

Lu X, Zoller EE, Weirauch MT, Wu Z, Namjou B, Williams AH, Ziegler JT, Comeau ME, Marion MC, Glenn SB et al. 2015. Lupus Risk Variant Increases pSTAT1 Binding and Decreases ETS1 Expression. *Am J Hum Genet* **96**: 731-739.

Ma CS, Nichols KE, Tangye SG. 2007. Regulation of cellular and humoral immune responses by the SLAM and SAP families of molecules. *Annu Rev Immunol* **25**: 337-379.

Mahot S, Sergeant A, Drouet E, Gruffat H. 2003. A novel function for the Epstein-Barr virus transcription factor EB1/Zta: induction of transcription of the hIL-10 gene. *J Gen Virol* **84**: 965-974.

Maier S, Staffler G, Hartmann A, Hock J, Henning K, Grabusic K, Mailhammer R, Hoffmann R, Wilmanns M, Lang R et al. 2006. Cellular target genes of Epstein-Barr virus nuclear antigen 2. *J Virol* **80**: 9761-9771.

Mannick JB, Cohen JI, Birkenbach M, Marchini A, Kieff E. 1991. The Epstein-Barr virus nuclear protein encoded by the leader of the EBNA RNAs is important in B-lymphocyte transformation. *J Virol* **65**: 6826-6837.

Maurano MT, Humbert R, Rynes E, Thurman RE, Haugen E, Wang H, Reynolds AP, Sandstrom R, Qu H, Brody J et al. 2012. Systematic localization of common disease-associated variation in regulatory DNA. *Science* **337**: 1190-1195.

McAllister K, Mechanic LE, Amos C, Aschard H, Blair IA, Chatterjee N, Conti D, Gauderman WJ, Hsu L, Hutter CM et al. 2017. Current Challenges and New Opportunities for Gene-Environment Interaction Studies of Complex Diseases. *Am J Epidemiol* **186**: 753-761.

McClellan MJ, Wood CD, Ojeniyi O, Cooper TJ, Kanhere A, Arvey A, Webb HM, Palermo RD, Harth-Hertle ML, Kempkes B et al. 2013. Modulation of enhancer looping and differential gene targeting by Epstein-Barr virus transcription factors directs cellular reprogramming. *PLoS Pathog* **9**: e1003636.

Mumbach MR, Rubin AJ, Flynn RA, Dai C, Khavari PA, Greenleaf WJ, Chang HY. 2016. HiChIP: efficient and sensitive analysis of protein-directed genome architecture. *Nat Methods* **13**: 919-922.

Murray RJ, Young LS, Calender A, Gregory CD, Rowe M, Lenoir GM, Rickinson AB. 1988. Different patterns of Epstein-Barr virus gene expression and of cytotoxic T-cell recognition in B-cell lines infected with transforming (B95.8) or nontransforming (P3HR1) virus strains. *J Virol* **62**: 894-901.

North KE, Howard BV, Welty TK, Best LG, Lee ET, Yeh JL, Fabsitz RR, Roman MJ, MacCluer JW. 2003. Genetic and environmental contributions to cardiovascular disease risk in American Indians: the strong heart family study. *Am J Epidemiol* **157**: 303-314.

Pender MP, Burrows SR. 2014. Epstein-Barr virus and multiple sclerosis: potential opportunities for immunotherapy. *Clin Transl Immunology* **3**: e27.

Pich D, Mrozek-Gorska P, Bouvet M, Sugimoto A, Akidil E, Grundhoff A, Hamperl S, Ling PD, Hammerschmidt W. 2019. First Days in the Life of Naive Human B Lymphocytes Infected with Epstein-Barr Virus. *mBio* **10**.

Quinlan AR, Hall IM. 2010. BEDTools: a flexible suite of utilities for comparing genomic features. *Bioinformatics* **26**: 841-842.

Rao SS, Huntley MH, Durand NC, Stamenova EK, Bochkov ID, Robinson JT, Sanborn AL, Machol I, Omer AD, Lander ES et al. 2014. A 3D map of the human genome at kilobase resolution reveals principles of chromatin looping. *Cell* **159**: 1665-1680.

Ricigliano VA, Handel AE, Sandve GK, Annibali V, Ristori G, Mechelli R, Cader MZ, Salvetti M. 2015. EBNA2 binds to genomic intervals associated with multiple sclerosis and overlaps with vitamin D receptor occupancy. *PLoS One* **10**: e0119605.

Rochford R, Moormann AM. 2015. Burkitt's Lymphoma. *Curr Top Microbiol Immunol* **390**: 267-285.

Saha A, Robertson ES. 2019. Mechanisms of B-Cell Oncogenesis Induced by Epstein-Barr Virus. *J Virol* **93**.

Schmidl C, Rendeiro AF, Sheffield NC, Bock C. 2015. ChIPmentation: fast, robust, low-input ChIP-seq for histones and transcription factors. *Nature methods* **12**: 963-965.

Schoenfelder S, Fraser P. 2019. Long-range enhancer-promoter contacts in gene expression control. *Nat Rev Genet* **20**: 437-455.

Schwartzberg PL, Mueller KL, Qi H, Cannons JL. 2009. SLAM receptors and SAP influence lymphocyte interactions, development and function. *Nat Rev Immunol* **9**: 39-46.

Serafini B, Rosicarelli B, Franciotta D, Magliozzi R, Reynolds R, Cinque P, Andreoni L, Trivedi P, Salvetti M, Faggioni A et al. 2007. Dysregulated Epstein-Barr virus infection in the multiple sclerosis brain. *J Exp Med* **204**: 2899-2912.

Servant N, Varoquaux N, Lajoie BR, Viara E, Chen CJ, Vert JP, Heard E, Dekker J, Barillot E. 2015. HiC-Pro: an optimized and flexible pipeline for Hi-C data processing. *Genome Biol* **16**: 259.

Shannon-Lowe C, Rowe M. 2011. Epstein-Barr virus infection of polarized epithelial cells via the basolateral surface by memory B cell-mediated transfer infection. *PLoS Pathog* **7**: e1001338.

Shao Z, Zhang Y, Yuan GC, Orkin SH, Waxman DJ. 2012. MAnorm: a robust model for quantitative comparison of ChIP-Seq data sets. *Genome Biol* **13**: R16.

Sullivan KD, Galbraith MD, Andrysik Z, Espinosa JM. 2018. Mechanisms of transcriptional regulation by p53. *Cell Death Differ* **25**: 133-143.

Tam V, Patel N, Turcotte M, Bosse Y, Pare G, Meyre D. 2019. Benefits and limitations of genome-wide association studies. *Nat Rev Genet* **20**: 467-484.

Vockerodt M, Cader FZ, Shannon-Lowe C, Murray P. 2014. Epstein-Barr virus and the origin of Hodgkin lymphoma. *Chin J Cancer* **33**: 591-597.

Wang C, Li D, Zhang L, Jiang S, Liang J, Narita Y, Hou I, Zhong Q, Zheng Z, Xiao H et al. 2019. RNA Sequencing Analyses of Gene Expression during Epstein-Barr Virus Infection of Primary B Lymphocytes. *J Virol* **93**.

Wang L, Grossman SR, Kieff E. 2000. Epstein-Barr virus nuclear protein 2 interacts with p300, CBP, and PCAF histone acetyltransferases in activation of the LMP1 promoter. *Proc Natl Acad Sci U S A* **97**: 430-435.

Wang Y, Song F, Zhang B, Zhang L, Xu J, Kuang D, Li D, Choudhary MNK, Li Y, Hu M et al. 2018. The 3D Genome Browser: a web-based browser for visualizing 3D genome organization and long-range chromatin interactions. *Genome Biol* **19**: 151.

Weintraub AS, Li CH, Zamudio AV, Sigova AA, Hannett NM, Day DS, Abraham BJ, Cohen MA, Nabet B, Buckley DL et al. 2017. YY1 Is a Structural Regulator of Enhancer-Promoter Loops. *Cell* **171**: 1573-1588 e1528.

Weirauch MT, Yang A, Albu M, Cote AG, Montenegro-Montero A, Drewe P, Najafabadi HS, Lambert SA, Mann I, Cook K et al. 2014. Determination and inference of eukaryotic transcription factor sequence specificity. *Cell* **158**: 1431-1443.

Wood CD, Veenstra H, Khasnis S, Gunnell A, Webb HM, Shannon-Lowe C, Andrews S, Osborne CS, West MJ. 2016. MYC activation and BCL2L11 silencing by a tumour virus through the large-scale reconfiguration of enhancer-promoter hubs. *Elife* **5**.

Wu DY, Krumm A, Schubach WH. 2000. Promoter-specific targeting of human SWI-SNF complex by Epstein-Barr virus nuclear protein 2. *J Virol* **74**: 8893-8903.

Zhao B, Maruo S, Cooper A, M RC, Johannsen E, Kieff E, Cahir-McFarland E. 2006. RNAs induced by Epstein-Barr virus nuclear antigen 2 in lymphoblastoid cell lines. *Proc Natl Acad Sci U S A* **103**: 1900-1905.

Zhao B, Zou J, Wang H, Johannsen E, Peng CW, Quackenbush J, Mar JC, Morton CC, Freedman ML, Blacklow SC et al. 2011. Epstein-Barr virus exploits intrinsic B-lymphocyte transcription programs to achieve immortal cell growth. *Proc Natl Acad Sci U S A* **108**: 14902-14907.

Zhou H, Schmidt SC, Jiang S, Willox B, Bernhardt K, Liang J, Johannsen EC, Kharchenko P, Gewurz BE, Kieff E et al. 2015. Epstein-Barr virus oncoprotein super-enhancers control B cell growth. *Cell Host Microbe* **17**: 205-216.

Zimber-Strobl U, Suentzenich KO, Laux G, Eick D, Cordier M, Calender A, Billaud M, Lenoir GM, Bornkamm GW. 1991. Epstein-Barr virus nuclear antigen 2 activates transcription of the terminal protein gene. *J Virol* **65**: 415-423.

Figure legends

Figure. 1. Schematic overview of the experimental design. Our working hypothesis is that EBNA2 alters human gene expression by rewiring the chromatin landscape. To test this hypothesis, RNA-seq, ChIP-seq, ATAC-seq, and HiChIP-seq experiments were performed in uninfected, EBV^{EBNA2-}-infected, and EBV^{EBNA2+}-infected Ramos B cells.

Figure 2. Differential gene expression in EBV-infected Ramos cells. Venn diagrams depicting the number of up-regulated genes (A) and down-regulated genes (B) based on comparisons between EBV^{EBNA2+} vs uninfected and EBV^{EBNA2-} vs uninfected conditions, respectively. Heatmaps indicate genes that are differentially expressed only in EBV^{EBNA2+} conditions.

Figure 3. EBNA2-dependent alteration of the human chromatin landscape. (*A*) EBNA2-dependent chromatin opening at the promoter of the upregulated EBNA2 DEG *NAALADL2-AS2*. UCSC Genome Browser screenshot (hg19) depicting binding of EBNA2 within the promoter region of *NAALADL2-AS2*, the most upregulated EBNA2 DEG. (*B,C*) EBNA2-dependent alteration of chromatin looping at the *SLAMF1* locus. (*B*) EBNA2-dependent looping to the promoter of the EBNA2 DEG *SLAMF1*. Loops outside of the window are not shown. (*C*) Extensive EBNA2-dependent rewiring of the chromatin looping landscape at the *SLAMF1* locus.

Figure 4. Intersection of EBNA2-dependent gene regulatory mechanisms and disease-associated genetic variants. The bar plot indicates the significance of the intersection (RELI negative $\log_{10}$ adjusted *p*-value). For all analyses, 176 diseases and phenotypes were tested. Only

diseases with at least one significant result (3 or more overlaps, corrected *p*-value < 0.05) are shown. Autoimmune diseases are indicated with red bars. Fold-enrichment and number of overlaps are indicated inside the bars. (*A*) Significant intersection between EBNA2-dependent differentially expressed genes and disease-associated variants ('Gain': upregulated genes; 'Loss': downregulated genes, relative to uninfected). (B) Significant intersection between EBNA2-dependent chromatin accessibility and disease-associated variants ('Gain': newly opened chromatin; 'Loss': newly closed chromatin, relative to uninfected). (C) Significant intersection between EBNA2-dependent chromatin looping and disease-associated variants ('Gain': new looping events; 'Loss': loss of looping events, relative to uninfected).

Figure 5. Allele-dependent and EBNA2-dependent mechanisms at autoimmune-associated genetic variants. UCSC Genome Browser shots (hg19) depicting EBNA2-based mechanisms at the *ZMIZ1* (A) and *CD80* (B) loci. Loops outside of the window are not shown (filtered). Red boxes indicate regions where EBNA2 binds in an allele-dependent manner. The ratio of reads between alleles is shown as a bar plot. See text for details.